



Influence of thiourea on the synthesis and characterization of chemically deposited nano structured zinc sulphide thin films

V. Padmavathy¹ · S. Sankar¹ · V. Ponnuswamy¹

Received: 27 September 2017 / Accepted: 13 February 2018 / Published online: 19 February 2018
© The Author(s) 2018. This article is an open access publication

Abstract

Nanocrystalline ZnS thin films incorporated onto glass substrates by chemical bath deposition method were investigated by X-Ray Diffraction (XRD), Atomic Force Microscopy (AFM), UV–Visible Spectroscopy (UV–Vis), Photoluminescence (PL), and Raman Spectroscopy (FT-R) studies. The influence of thiourea on the structural and optical properties of ZnS films was discussed in detail. The X-ray diffraction patterns confirmed the rhombohedral structure of ZnS thin films. AFM measurements indicated the nano carpet-like surface morphology variation in film with influence of thiourea. The optical absorption studies in the wavelength range of 200–800 nm showed that the band gap energy of ZnS has decreased from 3.69–3.36 eV, as thiourea varied from 0.2–0.8 M. The PL spectra divulged a shift near band edge emission around 360 nm, when thiourea concentration was increased. The Stokes shift calculations from PL emission spectra supported the relative intensities estimated from PL energy band spectra and showed a dependable repeatability for different molar concentrations. The Zn–S complexes were identified in the Raman spectra and the Raman spectral shift for 0.6 M composition of thiourea, which was found to be appreciable for ZnS thin films. The characterization studies clearly exposed the effect of thiourea onto the chemically deposited ZnS thin films.

1 Introduction

Zinc Sulphide (ZnS) belongs to a typical n-type semiconductor of II–VI semiconductors family [1–3]. It has a wide direct band gap of 3.6 eV and exciton binding energy of 40 meV at room temperature [4]. Because of its broad band gap energy, it is mostly used in blue shift light emitting diodes [5, 6]. Also, it is a promising material for future applications such as electroluminescent devices, displays, window layers of solar cells, solar and UV light emitting diodes, anti reflecting coatings, photovoltaic, and optoelectronic devices [7–11]. There are different techniques employed in the preparation of ZnS thin films, viz. electro deposition [12], pulsed laser deposition [13], spray pyrolysis [14], and chemical vapor deposition [15]. Among them, the chemical bath deposition (CBD) technique is more advantageous, since, it has simple methodology, ability to tune the optical properties of the films, and large area deposition [1]. The effect of different

substrates on the ZnS thin films was studied by Bacha et al. [16] and Daranfed et al. [17]. Lashgari et al. [18] investigated the electronic and optical properties of 2D ZnS and compared them with Wurtzite phase 3D ZnS using DFT calculations. In the present work, the authors focused on the preparation of nanocrystalline Zinc Sulphide thin films on glass substrate by using the chemical bath deposition method of different molar concentrations and their structural properties, surface morphology, particle size, and optical properties by using XRD, AFM, UV, PL, and FT-RAMAN studies, respectively were reported.

2 Experimental details

The stoichiometric nanocrystalline ZnS thin films were prepared by modified chemical bath deposition technique. The preparation process involved three steps, firstly, the substrate preparation, secondly, the synthesis of precursor solution, and thirdly, the ZnS film deposition.

✉ S. Sankar
drsankarsmit@gmail.com

¹ Condensed Matter Physics Laboratory, Department of Physics, Madras Institute of Technology, Anna University, Chennai, Tamil Nadu 600 044, India

2.1 Substrate preparation

The glass substrate (25 mm × 75 mm dimension) is used for film fabrication, since; it exhibits a maximum of 56% of transparency in visible light. Initially, the substrates were heated with concentrated chromic acid for 2 h and they were left at room temperature for 12 h. Then, the substrates were washed with acetone and rinsed with deionised water. Later, the clean glass slides were dipped into a beaker containing mixture solution. Finally, the setup is ready for film deposition.

2.2 ZnS precursor solution

Zinc nitrate [Zn(NO₃)₂] and thiourea [SC(NH₂)₂] were used as the source materials of Zn²⁺ and S²⁻ ions, respectively. Highly pure analytical grade reagent (99.97%) was used in the preparation of the samples. Along with Zinc nitrate solution, four different molarities (0.2, 0.4, 0.6 and 0.8) of thiourea solutions were prepared separately as given in Table 1. Each elemental solution was magnetically stirred for 30 min to form a homogeneous mixture. Then, the pH of precursors was well adjusted to 12 with ammonia solution using a pH meter. Lastly, these equimolar solutions were mixed together and stirred further for deposition of good quality films.

2.3 Nano film deposition

A paraffin oil bath was maintained at a constant temperature of 85 °C. The pretreated substrates have immersed into the bath to have thin film deposition for an hour. To enhance the incorporation of ions on substrate, a modified chemical bath deposition was carried out. It was accomplished by drop wise (25 drops/min) addition of ammonium nitrate solution and tri sodium citrate solution simultaneously into the precursor solution. The reaction solution was stirred during the deposition process. After the deposition, the substrate coated with ZnS films was washed with distilled water, and then, dried in open atmosphere, at room temperature, for 2 days. A typical synthesis of the film is shown as flow-chart in Fig. 1.

The reactions involved during the sample (films) deposition are as follows.

Reaction I: Zinc Nitrate with water for Zinc Nitrate decompositions:

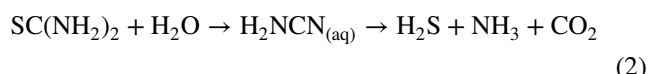
Zinc Nitrate + water → Zinc hydroxide + Nitric acid



Reaction II: Thiourea with water for Thiourea decompositions:

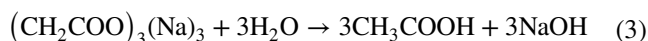
Thiourea + water → Intermediate compound

→ Hydrogensulphide + Ammonia + carbondioxide

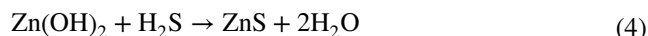


Reaction III: Trisodium citrate with water to speed up the reaction:

Trisodiumcitrate + water → Acetic acid + Sodium hydroxide



Final Reaction: Reaction I and II combines to form ZnS deposition



Water is a nucleophilic species and has a lone pair of electrons. The equations indicate the reaction against Zinc nitrate (Eq. 1), thiourea (Eq. 2) with the formation of intermediate compound that disintegrates to form the required ZnS products (Eq. 4). The reaction products of tri-sodium citrate with water (Eq. 3) were used to speed up the chemical reaction.

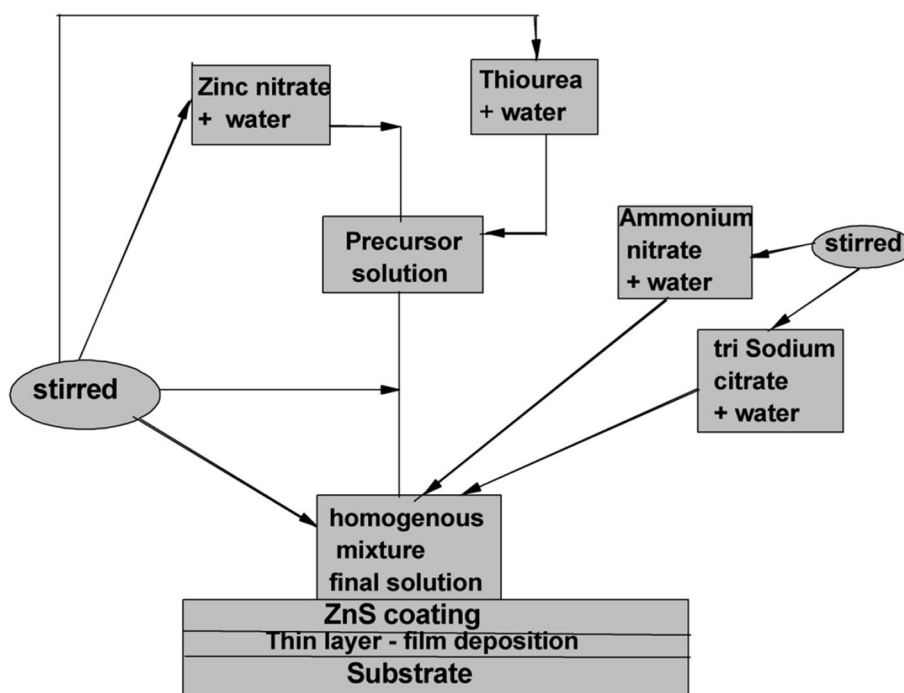
2.4 Characterization techniques

The powder XRD studies were carried out using a Rich-Seifert diffractometer with Cu Kα (λ = 1.5406 Å) radiation for 2θ values over 10°–70° for four different concentrations of thiourea in ZnS thin films. The 3D surface morphologies of ZnS thin films were compared with four different concentrations

Table 1 Details of samples synthesized and their assigned codes

| Samples number | Nominal composition in distilled water (H ₂ O) | | | | Sample code (M) |
|----------------|---|--|--------|------------------|-----------------|
| | Source materials | | Buffer | Complexing agent | |
| | Zn(NO ₃) ₂ (M/mL) | SC(NH ₂) ₂ (M/mL) | | | |
| 1 | 0.4/40 | 0.2/40 | 0.4/20 | 0.5/32 | 0.2 |
| 2 | 0.4/40 | 0.4/40 | 0.4/20 | 0.5/32 | 0.4 |
| 3 | 0.4/40 | 0.6/40 | 0.4/20 | 0.5/32 | 0.6 |
| 4 | 0.4/40 | 0.8/40 | 0.4/20 | 0.5/32 | 0.8 |

Fig. 1 Flow chart used to synthesis nano structured ZnS thin films



of thiourea using Atomic force microscopy (AFM, Digital Instrument, and Nanoscope III, USA). The transmission spectrum was recorded at room temperature using Shimadzu 1601 UV–Vis–NIR spectrophotometer in the range of 200–800 nm. The BRUKER RFS 27: Stand alone FT-Raman Spectrometer was used to measure the spectra in the range of 4000–50 cm^{-1} . The JY Fluorolog-3-11 fluorimeter provides optimum performance for both excitation and emission radiation in the range of 180–250 nm.

3 Results and discussion

3.1 Structural analysis

3.1.1 XRD studies

Powder X-ray diffraction analysis was carried out on thin films using the Cu $K\alpha$ radiation ($\lambda = 1.54060 \text{ \AA}$) Rich Seifert diffractometer. The recorded data were step scanned from 10° to 70° . The XRD patterns of as-deposited ZnS thin films onto the glass substrates with different molarities concentration are shown in Fig. 2. The standard JCPDS data file of ZnS XRD pattern is given as an insert in Fig. 2. The diffraction peaks of these ZnS thin films exhibit strong and weak non-discernible peaks. The observed diffraction lines corresponding to different planes indicated rhombohedral pattern which were confirmed by Saroj et al. [19] and Qutub et al. [20]. The result demonstrates that the diffraction peaks shifted to slightly higher 2θ value as given in Table 2.

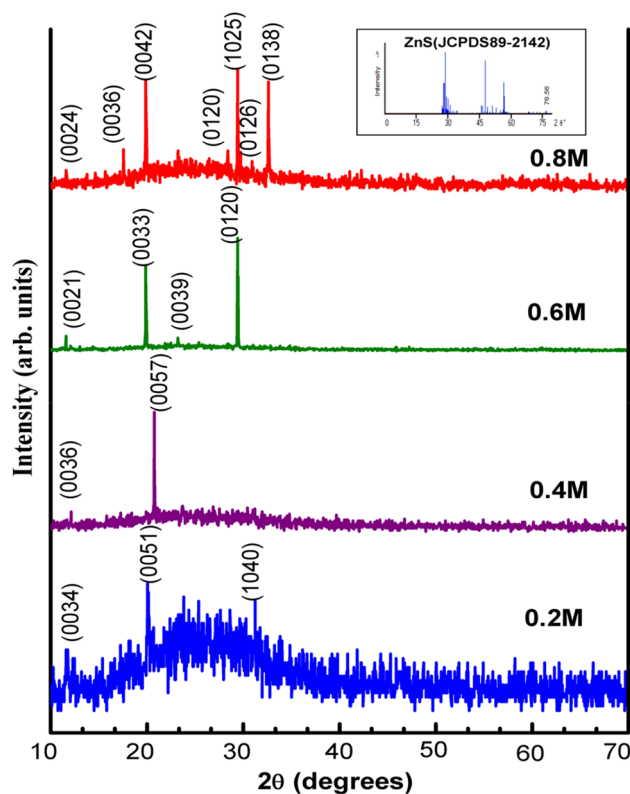


Fig. 2 XRD patterns of pure ZnS thin films

Table 2 Lattice parameters and particle size for different molar concentrations of ZnS thin films

| Conc. (M) | Structure | Cell parameters | | | Crystallite size D (nm) | 2 θ deg | Peaks (h k l) |
|-----------|--------------|-----------------|---|--------------|-------------------------|----------------|---------------|
| | | a | b | c | | | |
| 0.2 | Rhombohedral | 3.823 | | 224.92 μ | 64 | 20.12 | 0 0 51 |
| 0.4 | Rhombohedral | 3.823 | | 243.67 μ | 133 | 20.76 | 0 0 57 |
| 0.6 | Rhombohedral | 3.820 | | 150.24 μ | 163 | 29.48 | 0 1 20 |
| | | | | | | 19.89 | 0 0 33 |
| 0.8 | Rhombohedral | 3.823 | | 187.44 μ | 189 | 32.58 | 0 1 38 |
| | | | | | | 29.48 | 1 0 25 |
| | | | | | | 19.87 | 0 0 42 |

The XRD pattern hardly indicated any intense peak when the molar concentration was set to a low level of 0.2 M. However, the XRD pattern showed a single sharp peak when the molar concentration was increased to 0.4 M. Further, when the molar concentration was increased to 0.8 M, multiple sharp intense peaks appeared and were clearly visible. Thus, by increasing the molar concentration, the appearance of the number of sharp intense peaks increased. Therefore, it is established that the amorphous nature decreases with the increase in molar concentrations and improves the crystalline nature of the ZnS thin film. The XRD peaks observed in the present work were well defined for all molar concentrations as shown in Fig. 2. The predominance of the peak appearance of each case, confirmed the existence of the improved crystalline nature of the as-deposited films. Irrespective of the critical factors like annealing at different temperatures, thicknesses, multiple depositions, deposition time and nature of substrates, the appearance of increased number of intense, sharp, and multiple peaks at XRD pattern were very clear and it attributed to the present procedure of CBD. Such a clear XRD pattern has not been reported in the earlier studies made by Liu et al. [21], Ladar et al. [22], Sahraei et al. [23], and Zhou et al. [24]. All those studies reported about the existence of non discernible peaks for low thickness ZnS films.

Unlike the reports made by Long et al. [25] and Shin et al. [26], the present XRD results show rhombohedra structure with multiple discernible peaks of ZnS films and it is appreciably different from the reports of Shin et al. [27]. Though the increased numbers of well ladder, high intense peaks indicate the improved crystalline nature for 0.8 M, the XRD intensity for 0.6 M was more intense than that for 0.8 M due to the orientation of the nano-crystals along a single direction (0 1 20) plane for 0.6 M. It is further justified by employing AFM surface morphology observations. The absence of phases of ZnO or Zn(OH)₂ in the XRD pattern indicated the side reactions were restrained in the solution as reported by Liao et al. [28]. Also, the FT-Raman studies substantiated the obtained result. Further, it explicated the effect of annealing on ZnS thin films. With different annealing temperatures, Dalouji et al. [29] recorded special

deposition conditions to fabricate carbon–nickel films for electronic device applications. By annealing, the properties of the ZnS thin films change to ZnO films [4]. In order to retain the physical properties of the ZnS thin film, all the four samples were studied without annealing. Thus, Sulphur ions in thiourea play a crucial role in producing multiple peaks of XRD and indicating the crystalline nature of films. Similar results were reported by Arbi et al. [30] and Xu et al. [31] by using electro-deposition technique, Khomyak et al. [32] and Yoo et al. [33] by using RF magnetron sputtering method.

The mean crystalline size D is calculated using the Debye–Scherrer formula (Eq. 5)

$$D = K\lambda / \beta \cos 2\theta \quad (5)$$

where K is the geometric factor (0.9), λ is the wavelength of X-ray, β is the full width half maximum (FWHM), and θ is the angle of diffraction. The structural details and mean crystallite size (D) values are presented in Table 2. It is evident that, increasing the molar concentration from 0.2 to 0.8 M increases the particle size from 64 to 189 nm, as depicted in Table 2.

3.1.2 Atomic force microscopy (AFM) studies

The AFM studies gave the researchers an idea about the surface morphology of the as-deposited ZnS films. The nano carpet like patterns obtained for 0.2, 0.4, 0.6, and 0.8 M samples are shown in Fig. 3. Talu et al. [34] applied atomic force microscopy to characterize the 3D surface topographic features, particle size variation, and distribution of nanowires grown in an electric field.

The correlation between the size variations on grains by using the XRD patterns with that of the AFM study is portrayed in Fig. 3. The micrographs clearly reveal the effect of increasing thiourea concentration. The nanocrystals were not agglomerated and thus, the grains had grown in the same direction with uniform size for 0.6 M. Hence, based on this structural analysis, ZnS thin films for 0.6 M concentration of thiourea could be recommended for the optoelectronic device fabrications.

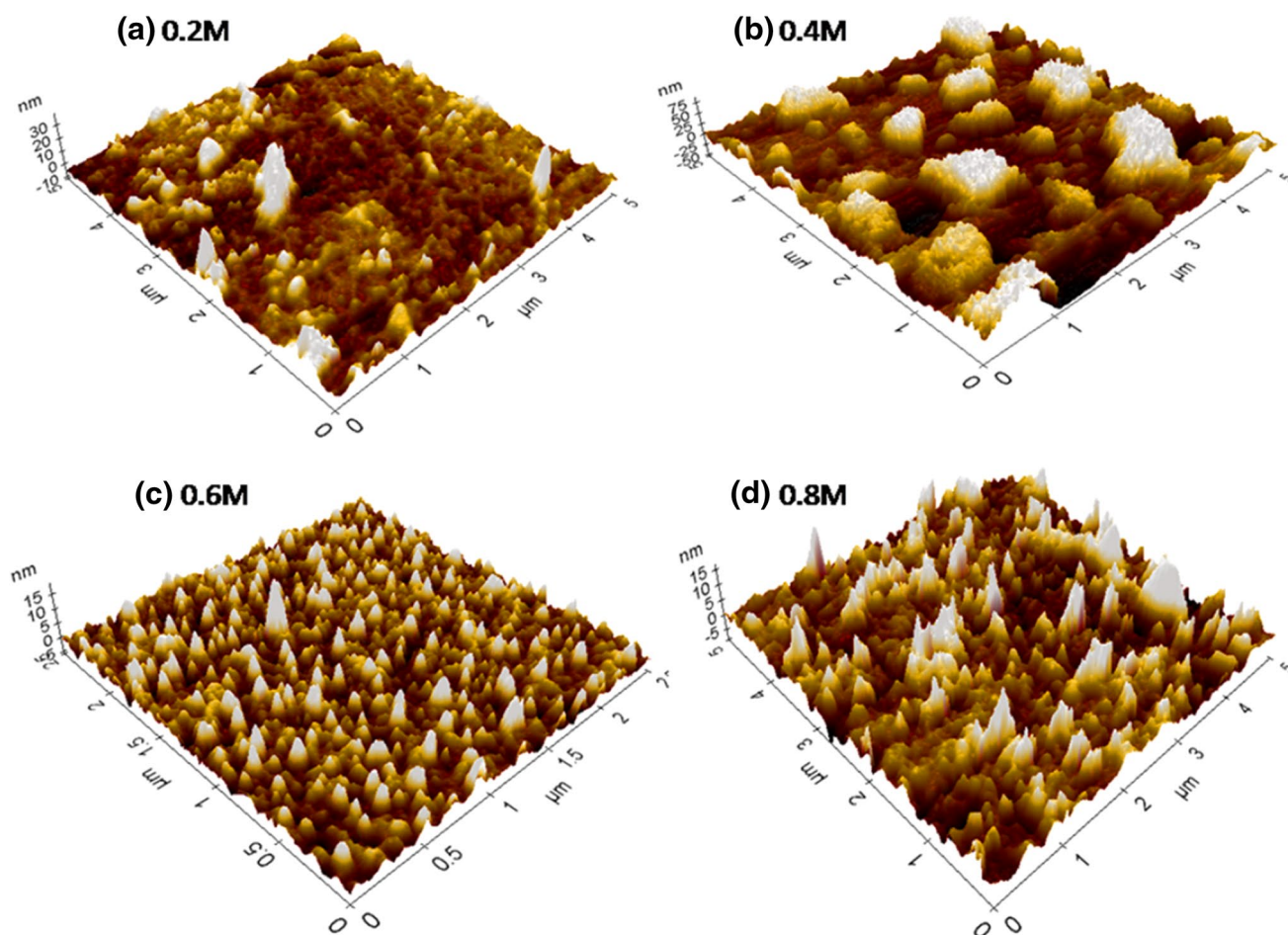


Fig. 3 The AFM morphologies for pure ZnS thin films deposited with different concentrations

3.2 Optical properties

The optical properties of the prepared films were studied by using the UV–Vis, photoluminescence, and Fourier Transform Raman spectroscopic measurements.

3.2.1 UV–Vis spectroscopy

The UV–Vis measurements of ZnS thin films deposited on glass substrates were made with the wavelength range of 200–800 nm. In order to have a clear picture about the variation of absorbance (%) with the wavelength (nm) for all the four different concentrations of thiourea, the region under discussions was enlarged (280–380 nm) and depicted as an inset (b) in Fig. 4. The Figure shows the absorption spectra of ZnS thin films for different molarities. Also, a range of sharp absorption edges was observed for different molarities of the ZnS deposited on the glass substrates.

From the spectra of Fig. 4, it can be observed that the absorbencies of the ZnS thin films were rapidly decreased up to 365 nm, after which it become stable above 400 nm.

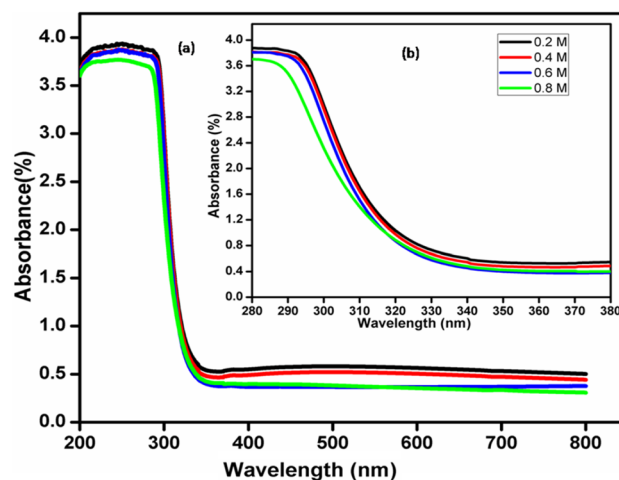


Fig. 4 The absorption spectra of pure ZnS thin films of different concentrations

With an annealed ZnS film, Doha et al. [35] observed sharp band edge absorption and reported that ZnS has a direct band gap. Similar type of results of ZnS films on glass substrates were reported earlier by Inamdar et al. [4] also. In the present work, a similar sharp absorption band edge of all the samples was observed, but without annealing. And hence, it can be considered that the as-deposited ZnS thin films have a direct band gap.

Using Tauc's relationship [36], the absorption coefficient (α) of ZnS can be correlated with band gap E_g and photon energy $h\nu$ as (Eq. 6)

$$\alpha h\nu = A(h\nu - E_g)^n \quad (6)$$

where A is a constant, n is $\frac{1}{2}$ for allowed direct transition, and E_g is the optical band gap. The E_g value is estimated by extrapolating linear part of $(\alpha h\nu)^2$ versus photon energy $h\nu$ plot to $\alpha h\nu = 0$. The Tauc plots of all the samples are shown in Fig. 5. The optical band gap (E_g) values obtained from these Tauc plots are presented in Table 3. The band gap was found to decrease with increasing molar concentration, as given in Table 3; for higher concentrations of thiourea, the energy gap has decreased considerably from that of the bulk (3.7 eV) [16, 37, 38].

The crystallite size was found to be increased with the increased molar concentration of thiourea, as given in Table 2. According to the reports of Bacha et al. [16], the glass substrate had a greater disorder which had influenced the optical band gap of the prepared film. In the present work, all the ZnS thin films were deposited on the glass substrates, so that; the reduction in the optical band gap can be well noticed with the concentrations.

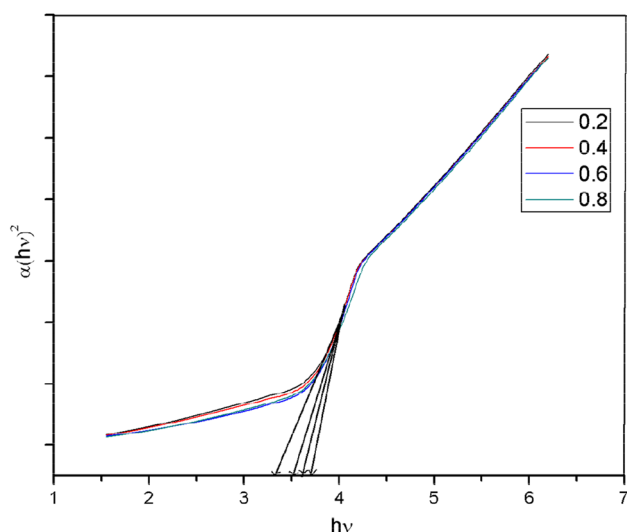


Fig. 5 Determination of band gap using $(\alpha h\nu)^2$ vs. $h\nu$

Table 3 Band gap determination using UV–Vis spectral studies in pure ZnS

| Conc. (M) | Wavelength (nm) | Bandgap (eV) |
|-----------|-----------------|--------------|
| 0.2 | 336 | 3.69 |
| 0.4 | 343 | 3.61 |
| 0.6 | 352 | 3.52 |
| 0.8 | 368 | 3.36 |

Goktas et al. [39] reported that the band gap had decreased from 3.59 to 3.23 eV upon increasing the Mn doping content, and Nasir et al. [40] observed that the optical band gap had decreased from 3.8 to 3.45 eV on increasing Al concentrations. In the present analysis, the absorbance peaks shifted to higher values of wavelength starting from 336 nm (0.2 M) to 368 nm (0.8 M), as given in Table 3. The decrease in the band gap was attributed to the appearance of S ions. The variation of energy band gap and crystallite size with different molar concentrations of thiourea in ZnS thin films are shown in Fig. 6. The band gap values obtained in the present study were in close agreement with those of Sahraei et al. [23].

3.2.2 Photoluminescence analysis

In order to investigate the effect of thiourea on the optical properties of ZnS thin layers deposited on the glass substrate, the photoluminescence measurements were employed. As photoluminescence spectroscopy provides information about the structure, band gap, impurity levels, and localized defects in semiconductors thin film [41], the room temperature photoluminescence spectra are recorded for ZnS thin films in the spectral range of 340–500 nm

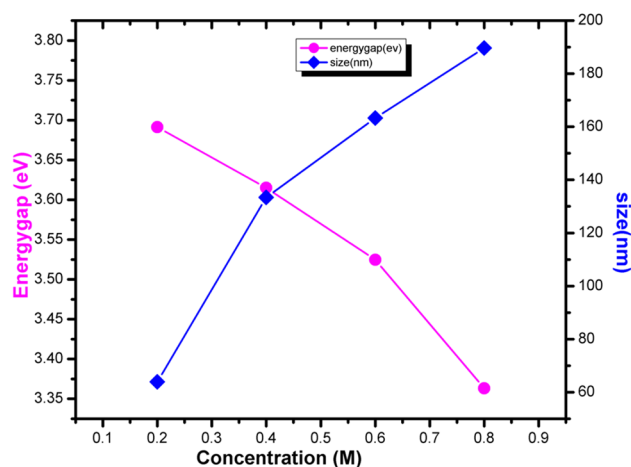


Fig. 6 Variation of energy bandgap and crystallite size with different molar concentrations of thiourea in ZnS thin films

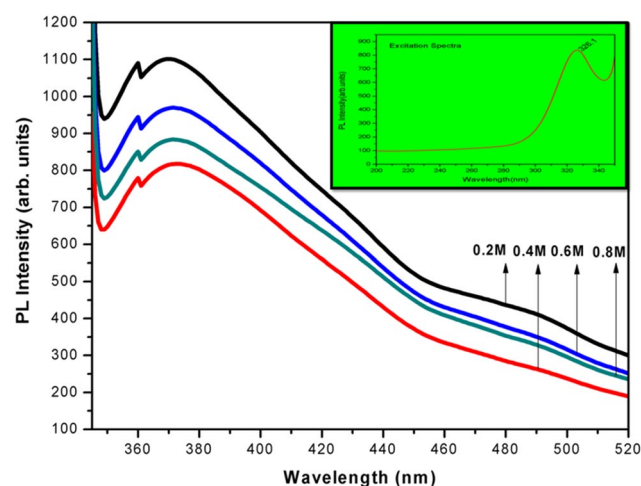


Fig. 7 Photoluminescence spectra of pure ZnS thin films deposited with different thiourea concentrations

with 325 nm excitation wavelength corresponding to photon energy of 3.8 eV, which is larger than the band gap of the ZnS thin films, and shown in Fig. 7. An insert of PL excitation spectra is included in the PL emission spectra to ensure that, for all the four samples, the PL measurements were carried out carefully with the same excitation wavelength. From the Fig. 7, two emission bands can be noticed for all the four samples with increase in the molar concentrations of thiourea. The PL emission is observed to be centred at 360 nm for 0.2 M of thiourea and it is centred around 359.9 nm for 0.6 and 0.8 M of thiourea. They were the near band emissions in the UV region which are the characteristic emission peaks of ZnS thin films [42, 43]. Adjacent to those characteristic band emission peaks, another emission peaks exists between 370 and 372 nm for all the molar concentrations of thiourea as given in Table 4. John et al. [44] reported that the PL emission peaks were observed at 388 and 398 nm which might be attributed to the band gap emission and that the strong band gap emission demonstrated high crystalline nature of the ZnS nano particles. In the present studies, a split in emission bands can be noticed in Fig. 7 PL spectra. The split in the emission bands is attributed to the spin–orbit coupling (‘s’ orbital—‘j’ orbital coupling in

the nano-crystalline ZnS thin films [42, 43]. Minute additional humps appeared around 400 nm in the blue emission region and close to 500 nm in the green emission (both the emissions are not apparent in Fig. 7) for 0.6 M. These humps (normally considered as weaker peaks) can be related to zinc vacancies and sulphur vacancies, respectively, as reported by Prathap et al. [45]. A similar kind of additional hump noticed around 489 nm for 0.8 M (not apparent in Fig. 7) can be associated with zinc interstitials [45]. The variation of PL emission peaks and the intensity of ZnS thin films for different molar concentrations of thiourea are given in Table 4. Over all, the non-existence of sharp appreciable peaks beyond 450 nm in the PL emission spectra depicted that the films synthesized were appreciably free from defects, dislocations, and impurities. The results have revealed that the prepared ZnS thin films for all the four samples have better quality and dependable crystalline nature.

The photoluminescence energy band spectra (Fig. 8a–d) are plotted from the PL emission spectra in the energy range of 2.1–3.6 eV and the results are summarized in Table 4. It is obvious, from Table 4, that there is a slight variation in energy band gap as the molarity of thiourea increased from 0.2 to 0.8 M. The emission energy band gap, E_{g1} varies only in the third decimal and beyond which implies that the variation of thiourea concentration has negligible effect on PL emission. This is again attributed to the reason that all the samples are with high purity and defect-free quality, as discussed above. The PL emission band gap results were found to be too close to the UV absorbance band gap results. Dejam et al. [46] observed increased PL emission intensities for AZO annealed films by reactive RF sputtering method. From Table 4, it is inferred that the relative intensities (RT1) increases from 0.6604 (0.2 M) to 0.8905 (0.8 M) and RT2 varied from 0.6680 (0.2 M) to 0.9275 (0.8 M). This is attributed to more number of electron–hole recombination occurrence in the low conduction band energy levels. Further, it is also clearly explained with Stokes energy shift in Table 4. The energy transfer during electron–hole recombination mainly depends on phonon participation. The difference in energy absorbed and energy emitted is the Stokes energy shift [47]. The energy will always be a lower value, because,

Table 4 The variation of PL peak positions with thiourea concentrations

| Conc. (%) (M) | PL emission (nm) P1, P2 | Energy gap (eV) E_{g1} , E_{g2} | Relative intensity (no unit) RT1, RT2 | Stokes shift Δ_{Stokes} (eV) |
|------------------|----------------------------|--|---|---|
| 0.2 | 360.06, 370.16 | 3.4438, 3.3499 | 0.6604, 0.6680 | 0.3715, 0.4654 |
| 0.4 | 360.01, 372 | 3.4444, 3.3333 | 0.6090, 0.6376 | 0.3715, 0.4888 |
| 0.6 | 359.91, 371.46 | 3.4453, 3.3381 | 0.6844, 0.7002 | 0.3700, 0.4772 |
| 0.8 | 359.91, 371.61 | 3.4453, 3.3368 | 0.8905, 0.9275 | 0.3700, 0.4785 |

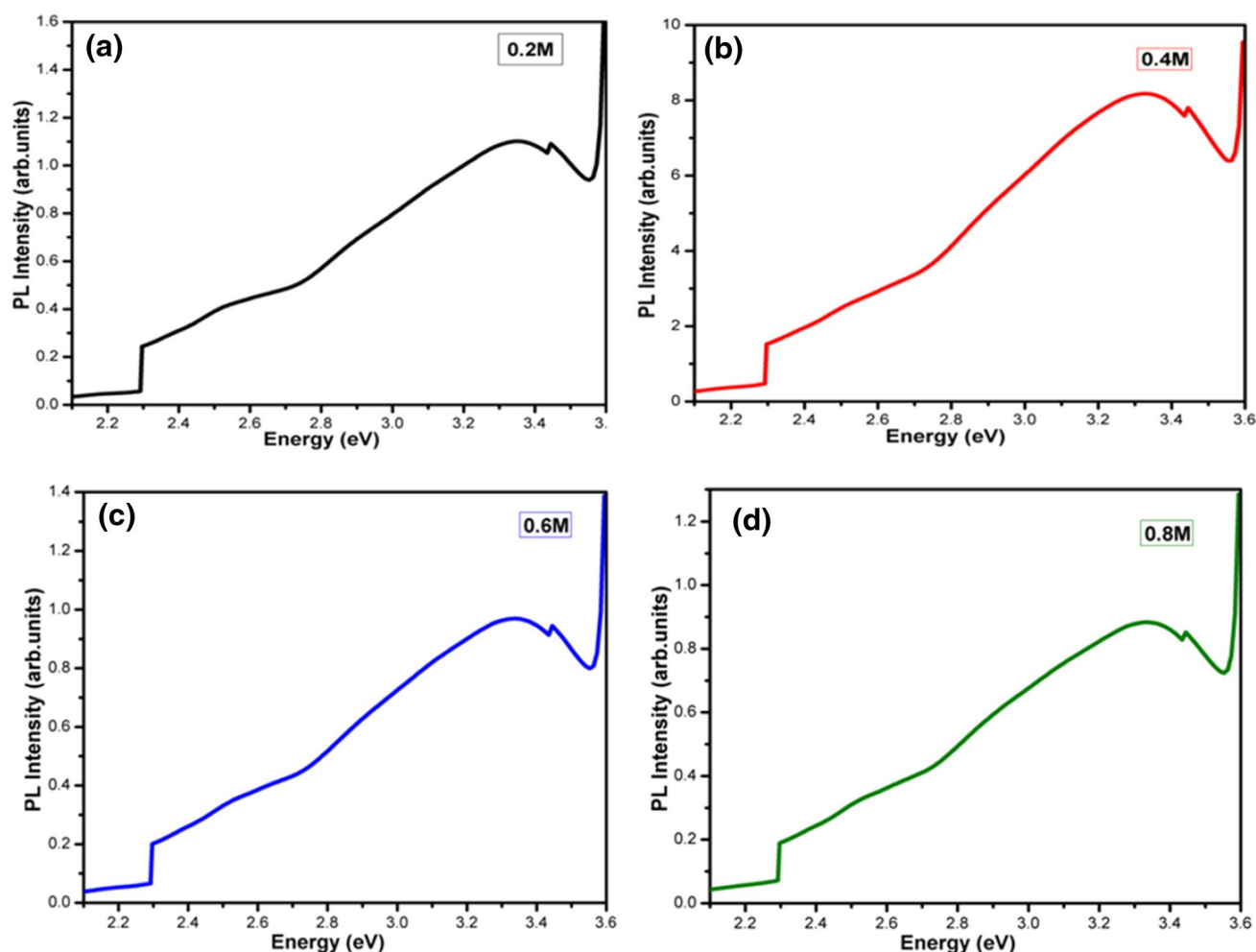


Fig. 8 Photoluminescence energy band spectra of ZnS films of different thiourea concentrations excited with 325 nm

according to the Stokes phenomenon [47], the energy emitted is always lesser than the energy absorbed. The Stokes energy shifts [41] were calculated using the Eq. (7) and it is tabulated in Table 4.

$$\Delta_{\text{stokes}}(\text{eV}) = E_{\text{g}} - E_{\text{PL}}(\text{eV}) \quad (7)$$

The values in Table 4 show meager shift in Stokes energy from 0.3715 eV (0.2 M) to 0.3700 eV (0.8 M) by increasing molar concentrations of thiourea. The main reason for these variations in Stokes energy can be attributed with phonon involvement in relaxation processes [41]. In addition, this behavior can be related to the non-radiative recombination of electron hole pairs present in the low conduction energy levels [41].

3.2.3 FT-RAMAN analysis

The information about the material composition, crystalline structure and lattice dynamics of a film were obtained

from Raman spectroscopy [48]. In the present study, Raman spectra have been used to reassert the presence of Zinc-rich and Sulphur-rich complexes with increasing thiourea concentrations and their effects on emission characteristics in the prepared ZnS thin films. Further, the existence of phonon modes by Stokes and anti-Stokes shifts were studied using Raman spectroscopy [28]. With regard to the literature, the peaks in the region of 300 cm^{-1} (strong) of 0.2, 0.4, 0.6, and 0.8 M correspond to transverse (TO) and longitudinal (LO) optical phonons of Zn-lattice [49, 50]. The film quality and vibrational properties of ZnS nano particles were analyzed using Raman Scattering at room temperature as shown in Fig. 9. The peaks near 664.74 cm^{-1} (0.2 M), 628.90 cm^{-1} (0.4 M), 871.18 cm^{-1} (0.6 M) and 603 cm^{-1} (0.8 M) are the characteristic vibrations of ZnS [51–53]. When compared to the other (0.2, 0.4, and 0.8 M) molar concentrations of thiourea, 0.6 M showed a much stronger ZnS characteristic vibrations (very Strong peak) from Raman spectra. Thus, it shows that 0.6 M of thiourea concentrations are highly

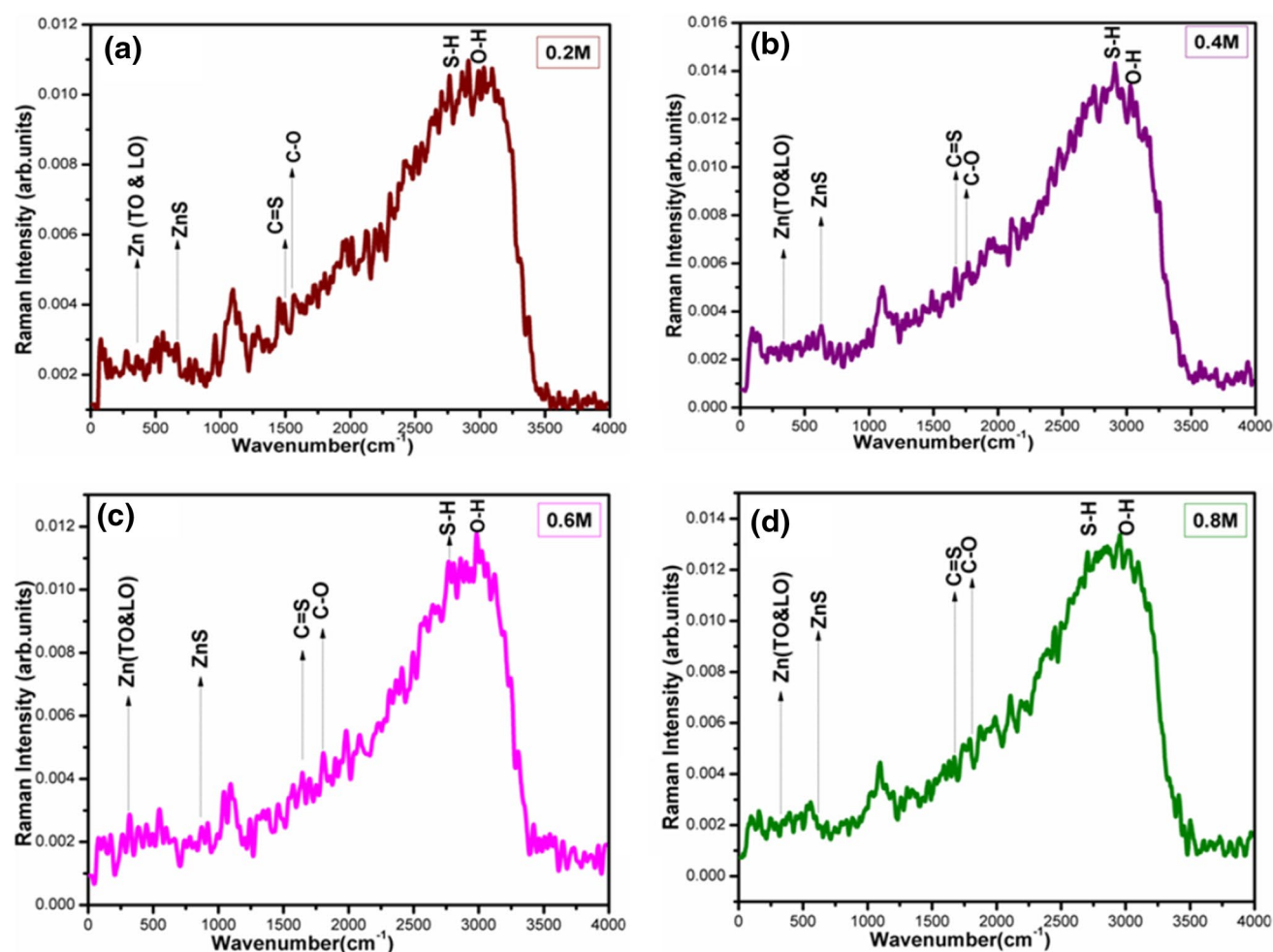


Fig. 9 Raman intense peaks for different concentrations of thiourea **a** 0.2 M, **b** 0.4 M, **c** 0.6 M, **d** 0.8 M

suitable for optoelectronic device applications. The presence of strong peaks at 2764 cm^{-1} (0.2 M), 2907 cm^{-1} (0.4 M), 2768 cm^{-1} (0.6 M), and 2705 cm^{-1} (0.8 M) corresponds to S–H stretching modes in thiourea [28]. The shift in Stokes energy in the Raman spectra from 2764 cm^{-1} (0.2 M) to 2705 cm^{-1} (0.8 M) of S–H modes was due to the increase in sulphur vacancies with the increase in thiourea concentrations [49]. All over, the FT Raman spectrum resembles FT-IR Spectrum [49] of ZnS thin films, and hence, the other peaks 1491 cm^{-1} (Strong-S) (0.2 M), 1671 cm^{-1} (S) (0.4 M), 1094 cm^{-1} (S) (0.6 M), 1198 cm^{-1} (weak-w) (0.8 M), correspond to C=S groups [28]. It was observed that the spectra assigned for C=S groups occur quite stronger in all the four molar concentrations of thiourea, which confirms the presence of sulphur complexes in the ZnS films. The peaks centered around 1569 cm^{-1} (w) (0.2 M), 1768 cm^{-1} (medium-m) (0.4 M), 1043 cm^{-1} (S) (0.6 M), 1141 cm^{-1} (w) (0.8 M), correspond to C–O bonds that exist on sodium citrate. The broad bands at 3029 cm^{-1} (S) (0.2 M), 3028 cm^{-1} (S) (0.4 M), 3121 cm^{-1} (S) (0.6 M), and 3178 cm^{-1} (w)

(0.8 M) correspond to –OH group of H_2O adsorbed on the surface of the film [7, 54]. Also, no additional peaks are observed for ZnO or $\text{Zn}(\text{OH})_2$ which indicates that all the four samples were studied instantly without annealing. In the present study, the results corresponded with XRD pattern analysis as discussed earlier. Thus, the structural analysis made by XRD and FT-Raman well establishes the fact that the prepared ZnS thin films were crystalline in nature without additional impurities.

4 Conclusion

Synthesis of ZnS thin films with different molar concentrations of thiourea was done by a modified chemical bath deposition technique at 85°C temperature and the structural and optical studies were carried out. The XRD studies showed improved crystalline nature of the ZnS thin films. However, ZnS thin films prepared with 0.6 M thiourea concentrations showed preferred growth along (0 1 20) direction

with higher intensity. The nanocrystallites of various sizes were observed as a three dimensional image using AFM. In particular, homogeneous nanoparticles with less agglomeration were observed for 0.6 M ZnS film. The UV–Vis spectra of ZnS film revealed a strong absorption edge due to the high crystalline nature. The band gap was found to be decreased with an increase in the thiourea concentration. The near band emission of PL spectra centred around 360 nm was observed for all the films with a noticeable Stokes shift that varies with molarity of thiourea. The absence of emission peaks in the visible region provided evidence for the lack of impurities and defects. The FT-Raman absorption spectra showed the characteristic peak in the finger print region of the ZnS from 664 to 871 cm^{-1} . The absence of ZnO vibrational modes in FT-Raman analysis confirmed the purity of ZnS in its pristine form.

Acknowledgements The authors are thankful to SAIF, IIT Chennai for PL and FT-RAMAN measurements, and the University of Madras, Chennai, for XRD facilities.

Open Access This article is distributed under the terms of the Creative Commons Attribution 4.0 International License (<http://creativecommons.org/licenses/by/4.0/>), which permits unrestricted use, distribution, and reproduction in any medium, provided you give appropriate credit to the original author(s) and the source, provide a link to the Creative Commons license, and indicate if changes were made.

References

1. A. Nabachandra Singh, L. Raghumani Singh, S. Nabadwip Singh, S. Bidyaswar Singh, Th. Ranjan Singh, Study of nanocrystalline ZnS thin films synthesized by CBD method. *Int. J. Nano Sci. Nanotechnol.* **4**, 1–6 (2013)
2. A.D. Dinsmore, D.S. Hsu, H.F. Gray, S.B. Qadri, Y. Tian, B.R. Ratna, Mn-doped ZnS nanoparticles as efficient low-voltage cathodoluminescent phosphors. *Appl. Phys. Lett.* **75**, 802–804 (1999)
3. R. Maity, K.K. Chattopadhyay, Synthesis and optical characterization of ZnS and ZnS:Mn nanocrystalline thin films by chemical route. *Nanotechnology* **15**, 812–816 (2004)
4. A.I. Inamdar, S. Lee, D. Kim, K.V. Gurav, J.H. Kim, H. Im, W. Jung, H. Kim, Metal-doped ZnS(O) thin films on glass substrates using chemical bath deposition. *Thin Solid Films* **537**, 36–41 (2013)
5. A. El Hichou, M. Addou, J.L. Bubendorff, J. Ebothe, B. Idrissi, M. Troyon, Microstructure and cathodoluminescence study of sprayed Al and Sn doped ZnS thin films. *Semicond. Sci. Technol.* **19**, 230–235 (2004)
6. R.H. Mauch, Electroluminescence in thin films. *Appl. Surf. Sci.* **92**, 589–597 (1996)
7. G. Nabiyouni, R. Sahraei, M. Toghiani, M.H. Majles Ara, K. Hedayati, Preparation and characterization of nanostructured ZnS thin films grown on glass and n-type Si substrates using a new chemical bath deposition technique. *Rev. Adv. Mater. Sci.* **27**, 52–57 (2011)
8. M. Bär, A. Ennaoui, J. Klaer, R. Sáez-Araoz, T. Kropp, L. Weinhardt, C. Heske, H.-W. Schock, Ch.-H. Fischer, M.C. Lux-Steiner, The electronic structure of the $[\text{Zn}(\text{S},\text{O})/\text{ZnS}]/\text{CuInS}_2$ heterointerface: impact of post-annealing. *Chem. Phys. Lett.* **433**, 71–74 (2006)
9. U. Gangopadhyay, K. Kim, D. Mangalaraj, J. Yi, Low cost CBD ZnS antireflection coating on large area commercial mono-crystalline silicon solar cells. *Appl. Surf. Sci.* **230**, 364–370 (2004)
10. S.H. Deulkar, C.H. Bhosale, M. Sharon, A comparative study of structural, compositional, thermal and optical properties of non stoichiometric $(\text{Zn},\text{Fe})\text{S}$ chalcogenide pellets and thin films. *J. Phys. Chem. Solids* **65**, 1879–1885 (2004)
11. H. Pang, Y. Yuan, Y. Zhou, J. Lian, L. Cao, J. Zhang, X. Zhou, ZnS/Ag/ZnS coating as transparent anode for organic light emitting diodes. *J. Lumin.* **122–123**, 587–589 (2007)
12. D. Gal, G. Hodes, D. Lincot, H.-W. Schock, Electrochemical deposition of zinc oxide films from non-aqueous solution: a new buffer/window process for thin film solar cells. *Thin Solid Films* **361–362**, 79–83 (2000)
13. S. Yano, R. Schroeder, B. Ullrich, H. Sakai, Absorption and photocurrent properties of thin ZnS films formed by pulsed-laser deposition on quartz. *Thin Solid Films* **423**, 273–276 (2003)
14. M.A. Hernández-Fenollosa, M.C. López, V. Donderisc, M. González, B. María, J.R. Ramos-Barradob, Role of precursors on morphology and optical properties of ZnS thin films prepared by chemical spray pyrolysis. *Thin Solid Films* **516**, 1622–1625 (2008)
15. D. Barreca, A. Gasparotto, C. Maragno, E. Tondello, C. Sada, CVD of Nanophasic (Zn, Cd)S thin films: from multi-layers to solid solutions. *Chem. Vapour Depos.* **10**, 229–236 (2004)
16. K.B. Bacha, A. Timoumi, N. Bitri, H. Bouzouita, Structural, morphological and optical properties of sprayed ZnS thin films on various substrate natures. *Optik* **126**, 3020–3024 (2015)
17. W. Daranf, M.S. Aida, A. Hafdallah, H. Lekiket, Substrate temperature influence on ZnS thin films prepared by ultrasonic spray. *Thin Solid Films* **518**, 1082–1084 (2009)
18. H. Lashgaria, A. Boochanib, A. Shekaaria, S. Solaymanic, E. Sartipib, R.T. Mendid, Electronic and optical properties of 2D graphene-like ZnS: DFT calculations. *Appl. Surf. Sci.* **369**, 76–81 (2016)
19. M.V. Saroj, M.P. Dharshini, V. Shally, G. Jayam, Structural, morphological, compositional and photoluminescent properties of CdS–ZnS nanocomposites synthesized by co-precipitation method. *Int. J. Res. Emerg. Sci. Technol.* **3**, 114–117 (2016)
20. N. Qutub, Synthesis and Characterization of nanomaterials, Ph.D. Thesis, Aligarh Muslim University. India 139, (2013)
21. J. Liu, A. Wei, Y. Zhao, Effect of different complexing agents on the properties of chemical-bath-deposited ZnS thin films. *J. Alloys Compd.* **588**, 228–234 (2014)
22. M. Lădar, E.-J. Popovici, I. Baldea, R. Grecu, E. Indrea, Studies on chemical bath deposited zinc sulphide thin films with special optical properties. *J. Alloys Compd.* **434–435**, 697–700 (2007)
23. R. Sahraei, G.M. Aval, A. Goudarzi, Compositional, structural, and optical study of nanocrystalline ZnS thin films prepared by a new chemical bath deposition route. *J. Alloys Compd.* **466**, 488–492 (2008)
24. L. Zhou, N. Tang, S. Wu, X. Hu, Y. Xue, Influence of deposition time on ZnS thin films performance with chemical bath deposition. *Phys. Procedia* **22**, 354–359 (2011)
25. F. Long, W.-M. Wang, Z. Cui, L.-Z. Fan, Z.-g. Zou, T.-k. Jia, An improved method for chemical bath deposition of ZnS thin films. *Chem. Phys. Lett.* **462**, 84–87 (2008)
26. S.W. Shin, S.R. Kang, J.H. Yun, A.V. Moholkar, J.-H. Moon, J.Y. Lee, J.H. Kim, Effect of different annealing conditions on the properties of chemically deposited ZnS thin films on ITO coated glass substrates. *Solar Energy Mater. Solar cells.* **95**, 856–863 (2011)

27. S.W. Shin, G.L. Agawane, M.G. Gang, A.V. Moholkar, J.-H. Moon, J.H. Kim, J.Y. Lee, Preparation and characteristics of chemical bath deposited ZnS thin films: effects of different complexing agents. *J. Alloys Compd.* **526**, 25–30 (2012)
28. J. Liao, S. Cheng, H. Zhou, B. Long, Al-doped ZnS thin films for buffer layers of solar cells prepared by chemical bath deposition. *Micro Nano Lett.* **8**, 211–214 (2013)
29. V. Dalouji, S. Elahi, S. Solaymani, A. Ghaderi, H. Elahi, Carbon films embedded by nickel nanoparticles: fluctuation in hopping rate and variable-range hopping with respect to annealing temperature. *Appl. Phys. A.* **122**, 541 (2016)
30. N. Arbi, I. Ben Assaker, M. Gannouni, A. Kriaa, R. Chtourou, Experimental investigation of the effect of Zn/S molar ratios on the physical and electrochemical properties of ZnS thin films. *Mater. Sci. Semicond. Process.* **40**, 873–878 (2015)
31. X. Xu, F. Wang, Z. Li, J. Liu, J. Ji, J. Chen, Effect of sulfosalicylic acid ($C_7H_6O_6S$) on the electrodeposition of pure ZnS nanocrystal thin films from acidic solutions. *Electrochim. Acta* **87**, 511–517 (2013)
32. V. Khomyak, I. Shteplyuk, V. Khranovskyy, R. Yakimova, Band-gap engineering of $ZnO_{1-x}S_x$ films grown by RF magnetron sputtering of ZnS target. *Vacuum* **121**, 120–124 (2015)
33. Y.Z. Yoo, Z.W. Jin, T. Chikyow, T. Fukumura, M. Kawasaki, H. Koinuma, S doping in ZnO film by supplying ZnS species with pulsed-laser deposition method. *Appl. Phys. Lett.* **81**, 3780–3798 (2002)
34. S. Talu, S. Solaymani, M. Bramowicz, S. Kulesza, A. Ghaderi, S. Shahpouri, S.M. Elahi, Effect of electric field direction and substrate roughness on three dimensional self-assembly growth of copper oxide nanowires. *J. Mater. Sci.: Mater. Electron.* **27**, 9272–9277 (2016)
35. M.H. Doha, M.J. Alam, J. Rabeya, K.A. Siddiquee, S. Hussain, O. Islam, M.A. Gafur, S. Islam, N. Khatun, S.H. Sarkar, Characterization of chemically deposited ZnS thin films on bare and conducting glass. *Optik* **126**, 5194–5199 (2015)
36. J. Tauc, *Amorphous Liquid Semiconductor*. (Plenum, New York, 1974)
37. T.B. Nasr, N. Kamoun, M. Kanzari, R. Bennaceur, Effect of pH on the properties of ZnS thin films grown by chemical bath deposition. *Thin Solid Films.* **500**, 4–8 (2006)
38. X.D. Gao, X.M. Li, W.D. Yu, Morphology and optical properties of amorphous ZnS films deposited by ultrasonic-assisted successive ionic layer adsorption and reaction method. *Thin Solid Films* **468**, 43–47 (2004)
39. A. Goktas, I.H. Mutlu, Room temperature ferromagnetism in Mn-doped ZnS nanocrystalline thin films grown by sol–gel dip coating process. *J. Sol–Gel Sci. Technol.* **69**, 120–129 (2014)
40. E.M. Nasir, Characterization of ZnS and ZnS:Al thin films. *Int. J. Adv. Res. Eng. Tech.* **4**, 266–275 (2013)
41. A. Jrad, W. Naffouti, T.B. Nasr, N. Turki-Kamoun, Comprehensive optical studies on Ga-doped ZnS thin films synthesized by chemical bath deposition. *J. Lumin.* **173**, 135–140 (2016)
42. M.M. David Kumar, S. Devadason, Phase transformation and quantum confinement effect in CdSe/Se multilayer thin films prepared by physical vapour deposition. *Phase Trans.* **86**, 1216–1226 (2013)
43. M.M. David Kumar, S. Devadason, Evidence for quantum confinement effects in CdSe/ZnSe multilayer thin films prepared by the physical vapor deposition method. *Acta Mater.* **61**, 4135–4141 (2013)
44. R. John, S. Sasi, Florence, optical, structural and morphological studies of bean-like ZnS nanostructures by aqueous chemical method. *Chalcogenide Lett.* **7**, 269–273 (2010)
45. P. Prathap, N. Revathi, Y.V. Subbaiah, K.T. Ramakrishna, K.R. Reddy, R.W. Miles, Preparation and characterization of transparent conducting ZnS:Al films. *Solid State Sci.* **11**, 224–232 (2009)
46. L. Dejam, S.M. Elahi, H.H. Nazari, H. Elahi, S. Solaymani, A. Ghaderi, Structural and optical characterization of ZnO and AZO thin films: the influence of post-annealing. *J. Mater. Sci.: Mater. Electron.* **27**, 685–696 (2016)
47. B. Ullrich, D. Ariza-Flores, M. Bhowmick, Intrinsic photoluminescence Stokes shift in semiconductors demonstrated by thin-film CdS formed with pulsed-laser deposition. *Thin Solid Films.* **558**, 24–26 (2014)
48. D.E. Ortiz-Ramos, L.A. Gonzalez, R. Ramirez-Bon, p-Type transparent Cu doped ZnS thin films by the chemical bath deposition method. *Mater. Lett.* **124**, 267–270 (2014)
49. J.W. Lee, C.-S. Hwang, White light emission from a colloidal mixture containing ZnS based nanocrystals: ZnS, ZnS:Cu and ZnS:Mn. *Bull. Korean Chem. Soc.* **35**, 189–196 (2014)
50. J. Schneider, R.D. Kirby, Raman scattering from ZnS polytypes. *Phys. Rev. B.* **6**, 1290–1294 (1972)
51. K. Nagamani, P. Prathap, Y. Lingappa, R.W. Miles, K.T.R. Reddy, Properties of Al-doped ZnS films grown by chemical bath deposition. *Phys. Proc.* **25**, 132–142 (2012)
52. H.F. Wang, Y. He, T.R. Ji, X.P. Yan, Surface molecular imprinting on Mn-doped ZnS quantum dots for room-temperature phosphorescence optosensing of pentachlorophenol in water. *Anal. Chem.* **81**, 1615–1621 (2009)
53. F. Gode, Annealing temperature effect on the structural, optical and electrical properties of ZnS thin films. *Phys. B.* **406**, 1653–1659 (2011)
54. G. Socrates, *Infrared Raman Characteristic Group frequencies*. (Wiley, New York, 2001)